AuCu Aerogels with Intriguing Surface Electronic Modulation as Highly Active and Stable Electrocatalysts for Oxygen Reduction and Borohydride Oxidation

Wang, Jiali; Chen, Fuyi; Jin, Yachao; Johnston, Roy L

DOI:
10.1002/cssc.201800052

License:
Other (please specify with Rights Statement)

Document Version
Peer reviewed version

Citation for published version (Harvard):
Wang, J, Chen, F, Jin, Y & Johnston, RL 2018, 'AuCu Aerogels with Intriguing Surface Electronic Modulation as Highly Active and Stable Electrocatalysts for Oxygen Reduction and Borohydride Oxidation', *ChemSusChem*. https://doi.org/10.1002/cssc.201800052

CHEMISTRY & SUSTAINABILITY

CHEMSUSCHEM

ENERGY & MATERIALS

Accepted Article

Title: AuCu Aerogels with Intriguing Surface Electronic Modulation as Highly Active and Stable Electrocatalysts for Oxygen Reduction and Borohydride Oxidation

Authors: Jiali Wang, Fuyi Chen, Yachao Jin, and Roy L Johnston

To be cited as: *ChemSusChem* 10.1002/cssc.201800052

Link to VoR: http://dx.doi.org/10.1002/cssc.201800052

A Journal of

ChemPubSoc Europe

WILEY-VCH

www.chemsuschem.org

AuCu Aerogels with Intriguing Surface Electronic Modulation as Highly Active and Stable Electrocatalysts for Oxygen Reduction and Borohydride Oxidation

Jiali Wang,[a] Fuyi Chen,*[a] Yachao Jin,[a] and Roy L. Johnston[b]

Abstract: We for the first time reported the successful synthesis of self-assembled AuCu aerogels via a one-pot kinetically-controlled approach. The startling electronic modulation effect of Cu on Au was observed across the entire alloy composition range, where the optimal upshift of d-band center for the highest activities was 0.24 eV. Due to the combination of nanoporous architecture and robust electronic effect, the $Au_{52}Cu_{48}$ aerogels exhibit more enhanced catalytic performance for oxygen reduction reaction (ORR) and direct borohydride oxidation reaction (BOR) compared to the commercial Pt/C catalysts. The specific and mass ORR activities on $Au_{52}Cu_{48}$ aerogels are 4.5 and 6.3 times higher than Pt/C, respectively, with negligible activity decay even after 10,000 cycles and 40,000 s duration. For BOR, the $Au_{52}Cu_{48}$ aerogels also exhibit far better selectivity and activity relative to Pt/C. The newly AuCu aerogels show great potentials as a promising alternative for Pt-based catalyst in fuel cells.

Introduction

Increasing environmental concerns and impending energy crisis caused by heavy reliance upon fossil fuels have driven the explosive research of sustainable clean energy technologies.[1] Fuel cells are among the most promising strategies to enable the direct conversion of chemical fuels to usable electrical energy without the emission of harmful pollutant.[2] Due to the sluggish kinetics of the cathodic reduction of oxygen and the anodic oxidation of fuels, the fuel cell performance is limited and strongly depends on the efficient catalysts to lower their electrochemical overpotential for high-voltage output.[3] Currently, platinum (Pt) is the state-of-the-art electrocatalyst for these reactions, however, its low earth abundance and high price seriously lead to the skyrocketing cost of fuel cell stacks.[4] Especially, the substantial activity degradation of Pt observed for both cathode and anode further hampers the practical large-scale implementation of fuel cells.[4a, 5] Therefore, developing cost-effective non-Pt catalysts with simultaneously high activity and superior stability is an open challenge and of tremendous significance for clean energy technologies.

Recently, Zhang and coworkers have reported the observed stabilization effect of Au clusters on Pt for oxygen reduction reaction (ORR), the resultant Au/Pt/C catalyst showed negligible activity degradation after 30,000 potential cycles under the oxidizing conditions,[6] which suggested that Au might have the great potential as an electrocatalyst with excellent durability. Unfortunately, the monometallic Au atoms are much less active than Pt atoms for ORR and the fuel oxidation reactions due to the weak adsorption of reactant molecules.[7] The strategies used to enhance the catalytic performance of monometallic Au are usually to alloy with 3d-transition metals to form Au-M (M=Ni,[8] Zn,[9] Cu[10]) bimetallic nanostructures and/or to reduce the size to increase the specific surface area.[11] These approaches have been demonstrated not only to effectively lower the total cost of Au-based catalysts but also to dramatically improve the catalytic activities. Among these inexpensive Au-M catalysts, Au-Cu alloys have shown promising potentials in CO_2 reduction,[12] hydrogen evolution reaction,[12a, 13] CO and glucose oxidation reactions.[14] Besides, the ordered AuCu intermetallic nanoparticles have also been researched as the alloyed cores in AuCu@Pt/Pd core-shell nanostructures for ORR, which effectively enhanced the mass activity of precious Pt/Pd by the strain and ligand effects.[15] However, there are only limited reports on the Au-Cu nanomaterials investigated as a direct electrocatalyst to catalyze ORR and borohydride oxidation reaction (BOR), and the latter is the important anodic reaction in the direct borohydride fuel cells. In few representative examples, Wang et al. employed the combined method of reduction and subsequent annealing to prepare the AuCu intermetallic nanoparticles supported on carbon black and investigated their activity for ORR, authors found that the AuCu/C intermetallic nanoparticles showed a clearly higher activity relative to Au/C nanoparticles.[16] Zhang et al. further synthesized the $AuCu_3$/C intermetallic nanoparticles by a similar complex method, these intermetallics exhibited enhanced catalytic activity than both the intermetallic AuCu/C and Au/C nanoparticles for ORR.[17] However, the activities of these ordered intermetallic nanoparticles towards ORR were still inferior to the commercial Pt/C catalysts in terms of the half-wave potential. And the electrochemical stability of Au-Cu intermetallics, especially under long-term potential cycling including high potentials, was also reported to be far from satisfactory.[17] Moreover, it can be noted that these previous studies have mainly focused on the ordered Au-Cu intermetallic nanoparticles that are characteristic of the fixed atomic ratio and limited sphere shape, with rare studies on the Au-Cu random nanoalloys for ORR. Solid solution nanoalloy phases, with broadly-tunable compositions, diverse morphologies and usually synthesized using the mild strategies,

[a] Dr. J. Wang, Prof. F. Chen, Dr. Y. Jin
State Key Laboratory of Solidification Processing
Northwestern Polytechnical University
Xi'an 710072, China
E-mail: fuyichen@nwpu.edu.cn
[b] Prof. R. L. Johnston
School of Chemistry
University of Birmingham
Birmingham B15 2TT, U.K.

Supporting information for this article is given via a link at the end of the document.

provide more flexible control over structural and electronic effects not afforded by the ordered intermetallic phases.[12a] Thus, the urgent exploit of developed Au-Cu nanoalloys with remarkably improved catalytic activity together with excellent stability for both ORR and BOR is highly required to make them be more competitive with state-of-the-art Pt-based electrocatalysts.

Herein, we report a new class of AuCu aerogels self-assembled through a versatile one-pot kinetically-controlled strategy. The modulation effect of Cu atoms on the Au is found to effectively induce an upshift of the d-band center in the Au-Cu nanoporous aerogels within the entire alloy composition range, as evidenced by X-ray photoelectron spectroscopy (XPS) measurement. This electronic effect is startling because the electronegativity of Cu (1.9) is lower than that of Au (2.4) and it is expected that the charge transfer from Cu to Au lowers the d-band center of Au in the Au-Cu nanoalloys. Such intriguing electronic interactions between Cu and Au render the AuCu aerogels with more-active catalytic sites, in addition to a hierarchically porous architecture, as a high performance bifunctional electrocatalyst for fuel cell reactions. The optimal d-band center upshift of 0.24 eV with respect to pure Au was observed on $Au_{52}Cu_{48}$ aerogels, which translated to the highest activity for both ORR and BOR among Au-Cu systems reported in the literature, and even the commercial Pt/C catalysts. Compared to Pt/C, the $Au_{52}Cu_{48}$ aerogels show a positive shift of 42 mV in half-wave potential, and their performance reaches up to 4.5 and 6.3 times improved specific and mass activity (0.906 mA cm^{-2} and 0.960 A mg^{-1}_{Au}) for ORR, respectively. Most impressively, the long-term stability test demonstrates their outstanding durability with 95.8 % mass activity maintained after 10,000 potential cycles. Moreover, the $Au_{52}Cu_{48}$ aerogels also show a much higher selectivity and activity for BOR relative to the Pt/C. The general and versatile synthetic strategy in our work can be easily extended to develop other novel bi/multi-metallic systems. It is believed that the insights gained through this study might provide more opportunities to design more high-performance non-Pt catalysts for sustainable energy applications.

Results and Discussion

The bimetallic AuCu aerogels were first synthesized via a facile one-step reduction process mediated by a strong reducing agent (sodium borohydride) at room temperature and followed by the freeze drying. Such kinetically-controlled synthetic process was significantly simplified compared with the traditional synthesis for aerogels due to the elimination of concentration step.[18] The morphologies and structures of the resultant products were investigated by scanning electron microscopy (SEM) and transmission electron microscopy (TEM). As seen in Figure 1a-b, the obtained $Au_{52}Cu_{48}$ bimetallic aerogels possess a typical 3D sponge-like architecture made up of porous, interconnected networks. Higher magnification image in Figure 1c reveals that, unlike the agglomerated structures composed of single nanoparticles well-separated from each other, the $Au_{52}Cu_{48}$

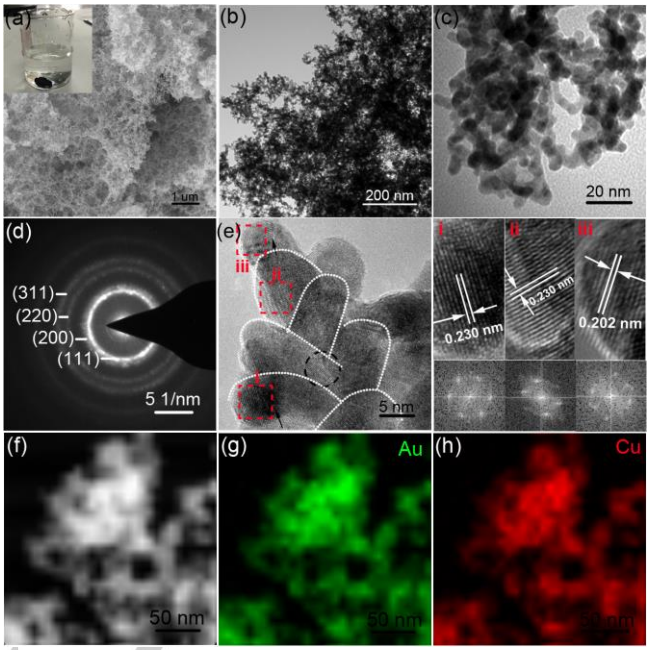

Figure 1. General physical characterizations of the as-synthesized $Au_{52}Cu_{48}$ aerogels electrocatalyst. (a) SEM image, the inset in (a) shows the optical photo of the $Au_{52}Cu_{48}$ aerogels, confirming the formation of fluffy black solid out of the $NaBH_4$ solution by using a one-step method at room temperature. (b, c) Bright field TEM images. (d) SAED pattern. (e) HRTEM image of several branches composed of highly crystalline fused nanoparticles. (i-iii) Magnified HRTEM images and the corresponding Fast Fourier Transform (FFT) patterns obtained from regions i, ii and iii marked by squares in (e). (f) HAADF-STEM image. (g-h) High-resolution STEM-EDX elemental mapping images of the $Au_{52}Cu_{48}$ aerogels for (g) Au and (h) Cu, showing the uniform distribution of Au and Cu elements.

aerogels display a wire-like morphology with many branches through the fusion of fine nanoparticles with the diameter of about 6-10 nm. A great number of pores and channels created by the interconnected branches were also observed, which effectively improves the utilization of noble metal and offers an open 3D structure for molecular accessibility during the catalytic process. It can be deduced that the kinetically-controlled reduction of the metal precursors with a strong reducing agent creates massive bare metal nuclei in a short time and then provides the nucleation sites for nanoparticles growth, which acts as basic building blocks for the 3D AuCu aerogels. The rapid fusion and growth of these bare metallic nanoparticles induces the formation of fluffy black solid out of the solution within three minutes at room temperature (inset in Figure 1a). Besides, the effervescence can readily form during the synthetic process due to the release of H_2, which also help to create the hierarchical pores in AuCu aerogels.[19] The typical selected-area electron diffraction (SAED) pattern recorded from the branches shown in Figure 1c clearly displays the continuous diffraction rings that can be indexed to the (111), (200), (220), and (311) planes of the face-centered cubic (fcc) polycrystalline structure (Figure 1d). Figure 1e shows the high-resolution TEM (HRTEM) image to further illustrate the detailed structural features of $Au_{52}Cu_{48}$ aerogels. It can be seen that several crystalline

domains with the specific lattice planes are clearly distributed on each branch (marked by the black arrows and broken circle), which convincingly confirms that the networks originate from the fused nanoparticles. The HRTEM images of three randomly selected nanoparticles are highly crystalline with clear continuous lattice fringes, indicating the single-crystalline nature of the fused nanoparticles, as could further be proved by the corresponding Fast Fourier Transformation (FFT) patterns. The interplanar spacing is about 0.230 and 0.202 nm, matching the in-between values of the (111) and (200) planes of the metallic fcc Au and Cu, respectively, suggesting the fully alloyed nature of the $Au_{52}Cu_{48}$ aerogels. The high-angle annular dark field scanning transmission electron microscope (HAADF-STEM) in Figure 1f exhibits that the $Au_{52}Cu_{48}$ aerogels are composed of the 3D nanopores and channels (dark region). The corresponding energy dispersive X-ray (EDX) spectroscopy (Figure 1g-h) clearly shows that both Au and Cu are uniformly distributed throughout the networks, which confirms the formation of homogenous bimetallic nanoalloys after the simultaneous reduction with sodium borohydride, leading to the robust atomic interaction and superior catalytic performance. The most important feature of the present synthetic strategy is its high generality for the preparation of bimetallic or pure monometallic nanoporous structures by simply changing the metal precursors. The SEM images of the pure monometallic Au, Cu and other AuCu aerogels with different compositions were presented in Figure S1. As expected, all the samples reveal almost the same morphologies, indicating the little effect of alloying composition on the morphology and the important versatility of this facile method.

The EDX analysis in Figure S2 exhibits that the Au/Cu atomic ratio is about 1.1 (52:48) for the $Au_{52}Cu_{48}$ aerogels, which is in good agreement with the feeding ratio in the initial precursor (Au^{3+}/Cu^{2+}= 1:1). Most intriguingly, the composition tunability of the resultant AuCu aerogels could be easily achieved through adjusting the mole ratio of precursors during the synthetic process. When the ratios of Au^{3+} and Cu^{2+} in the precursor were altered to 3:1, 2:1, 1:2 and 1:3, the $Au_{74}Cu_{26}$, $Au_{65}Cu_{35}$, $Au_{32}Cu_{68}$, and $Au_{25}Cu_{75}$ aerogels were observed (insets in Figure S1 and Table S1), respectively. It can be concluded that the kinetically-controlled complete reduction process in the excess $NaBH_4$ solution results in the precise control of the alloy composition. The N_2 adsorption-desorption isotherm was performed to analyze the surface area and porosity property of the $Au_{52}Cu_{48}$ aerogels. The surface area as estimated by using the Brunauer-Emmett-Teller (BET) method is 38.4 m^2 g^{-1}, which is considerably larger than that of porous Au-based materials by using other synthetic method.[20] The porosity at the nanoscale resulting from the fusion of metal nanoparticles emerged during the nucleation step might contribute to the higher BET surface area. As shown in Figure S3a, the physisorption isotherm exhibits a type II behavior that is characteristic for typical macroporous structures (pore diameter > 50 nm).[21] The pore size distribution of the $Au_{52}Cu_{48}$ aerogels (Figure S3b) based on the Barrett-Joyner-Halenda (BJH) theory shows the presence of a broad range of pores from micropores (< 2 nm) to mesopores (2-50 nm). In addition, it can be noted that the mesopores and

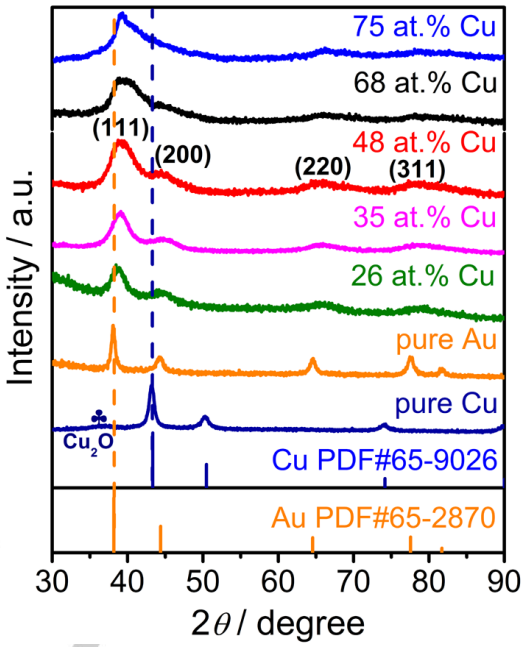

Figure 2. XRD patterns of different AuCu aerogels electrocatalysts alongside with pure monometallic Au and Cu samples, Bar diagram: Au #65-2870, Cu #65-9026.

macropores dominated the porosity of $Au_{52}Cu_{48}$ aerogels according to the cumulative pore volume analysis together with the results of TEM characterizations. Such hierarchical porosity system in the $Au_{52}Cu_{48}$ aerogels effectively facilitates the mass transportation and offers more reaction sites for the reactants in the catalysis.

The crystalline structures of the different AuCu, monometallic Au and Cu aerogels were analyzed by X-ray diffraction (XRD). As shown in Figure 2, all the lattice plane diffraction peaks of the AuCu aerogels are located between the peaks of pure fcc Au (JADE PDF. No. 65-2870) and Cu (JADE PDF. No. 65-9026). Although a thin oxide shell was found in the pure Cu sample according to its XRD data, it is noteworthy that there are no characteristic peaks corresponding to Cu or Cu oxide observed in the AuCu aerogels patterns. These collective results fully illustrate the formation of a highly crystalline AuCu bimetallic nanalloys rather than a mixture of separated gold and copper, as well as the excellent oxidation resistance of the AuCu aerogels by the presence of Au in the nanoalloys. The representative diffraction peaks at 39.2°, 44.8°, 65.9° and 78.7° in the $Au_{52}Cu_{48}$ aerogels catalyst pattern can be readily indexed to (111), (200), (220), and (311) reflections of the fcc-structured AuCu solid solution nanoalloys, which matches well with the SAED pattern. Additionally, the broad diffraction peaks also confirm the ultrathin feature of fused nanoparticles in the $Au_{52}Cu_{48}$ aerogels. According to the Debye-Scherrer equation, d = 0.89 λ/(β cosθ), where λ refers to the wavelength of X-ray, β denotes the peak width at half-maximum, and θ is the Bragg angle, the XRD peak of (111) gives the mean nanoparticles size of ~5 nm, consistent with the results obtained from the HRTEM image (Figure 1e). It

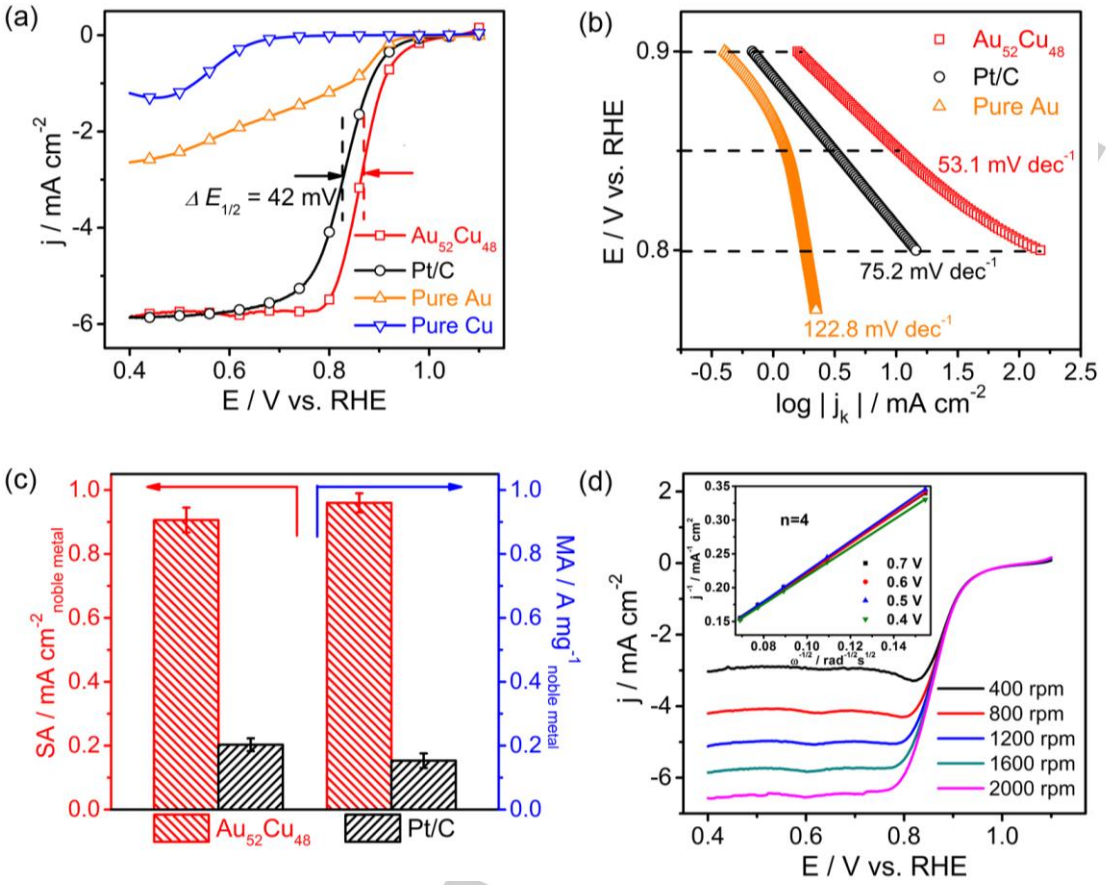

Figure 3. The electrochemical characterizations of various catalysts recorded in O_2-saturated 0.1 M KOH solution with a sweep rate of 10 mV s^{-1} and the RDE rotation rate of 1600 rpm. (a) ORR polarization curves of $Au_{52}Cu_{48}$ aerogels (red line), the commercial Pt/C (black line), pure Au (orange line) and pure Cu (blue line) catalysts. (b) Comparative mass-corrected Tafel plots of $Au_{52}Cu_{48}$ aerogels, the Pt/C and pure Au catalysts. (c) The comparison of ORR specific activity (SA) and mass activity (MA) of $Au_{52}Cu_{48}$ aerogels and the Pt/C catalysts at 0.85 V vs. RHE. (d) ORR polarization curves of $Au_{52}Cu_{48}$ aerogels at different rotation rates. The inset shows the corresponding Koutecky-Levich plots (j^{-1} vs. $\omega^{-1/2}$) at different potentials. The electrocatalytic results are obtained from at least three independent measurements, and the error bars are also included in (c). In (a) and (d), current densities are normalized by the geometric area of a RDE (0.196 cm^2).

can be further concluded that the interconnected nanowire with the diameter of 6-10 nm is composed of the coalescence of single nanocrystallite.

For bi/multi-metallic nanostructures, the "clean" reactive surfaces, degree of alloying and well-controlled composition are very important features for electrocatalytic activity. In this work, we successfully excluded the use of any stabilization agents, which makes the "clean" functional metal surfaces easily accessible to the reactant molecules. Most importantly, the fully alloyed AuCu bimetallic aerogels with uniformly distributed elements and precisely controlled compositions can be facilely gained through the complete co-reduction of different metal ions. These results exhibit some significant improvements in the synthetic route compared with that reported by the previous research,[22] in which the separated phases with the composition deviation and organic species residuals were usually observed. The favorable features in our synthesis allow the design of a catalyst with optimum balance among composition, activity and durability, and facilitate to fully exploit the synergistic effects between different metals in improving the catalytic activity.

The electrocatalytic ORR performance of AuCu aerogels catalyst was first examined and compared with that of a benchmark Pt/C catalyst and pure metal components under identical conditions. The linear sweep voltammetry (LSV) curves were recorded in O_2-saturated 0.1 M KOH solution at the rotation rate of 1600 rpm. As shown in Figure 3a, it can be seen that the $Au_{52}Cu_{48}$ aerogels catalyst has a considerably higher ORR activity than that of the commercial Pt/C or pure monometallic catalysts. For example, in the kinetic-diffusion region, a more positive onset potential (E_{onset}) was observed on the $Au_{52}Cu_{48}$ aerogels (1.000 V) compared with the commercial Pt/C (0.964 V). Moreover, the half-wave potential ($E_{1/2}$) of $Au_{52}Cu_{48}$ aerogels catalyst (0.868 V) shows a significantly positive shift of 42 mV relative to that of the Pt/C (0.826 V) (Table S2), indicating the substantial ORR activity at lower overpotentials. The enhanced ORR activity is further confirmed by the mass transport corrected Tafel plots in Figure 3b. The

kinetic current of $Au_{52}Cu_{48}$ aerogels catalyst is the highest among the three different catalysts at the low overpotential regime (> 0.85 V). On the other hand, the $Au_{52}Cu_{48}$ aerogels catalyst presents a Tafel slope of 53.1 mV dec^{-1} in comparison to 75.2 and 122.8 mV dec^{-1} for the Pt/C and pure Au catalysts, respectively. The smaller Tafel slope of $Au_{52}Cu_{48}$ aerogels catalyst indicates its superior ORR performance than other two catalysts due to the facile oxygen adsorption and subsequent reduction reaction.[23] The LSV curves and Tafel plots for the other AuCu aerogels catalysts alongside with the Pt/C reference catalyst were compared in Figure S4. The electrochemically active surface areas (ECSAs) of $Au_{52}Cu_{48}$ aerogels and the commercial Pt/C catalysts according to the typical cyclic voltammetry (CV) are calculated to be 106 m^2 g^{-1}_{Au} and 75 m^2 g^{-1}_{Pt}, respectively (Figure S5). We have also synthesized the AuCu/C intermetallic NPs according to the method reported by Zhang et al.[17] From the TEM image in Figure S5a, the as-synthesized AuCu intermetallic NPs are uniformly distributed on the carbon black. The calculated ECSA of AuCu/C intermetallic NPs is 69.2 m^2 g^{-1}_{Au}, which is smaller than that of $Au_{52}Cu_{48}$ aerogels. The rather high ECSA of the $Au_{52}Cu_{48}$ aerogels is mainly due to the geometrical advantage of hierarchical porosity system, which would facilitate to expose more Au active sites on the surface to promote the catalytic activity. Then, the specific activity (SA) and mass activity (MA) of $Au_{52}Cu_{48}$ aerogels and commercial Pt/C catalysts were further evaluated, where the kinetic currents were normalized by the ECSA and the loading amount of noble metals, respectively (The kinetic current was calculated by the Koutecky-Levich equation). As shown in Figure 3c, the $Au_{52}Cu_{48}$ aerogels catalyst exhibits a SA of 0.906 mA cm^{-2} at 0.85 V, which is about 4.5 times higher than that of the commercial Pt/C catalyst (0.203 mA cm^{-2}). On the basis of the mass loading of noble metals, the MA of the $Au_{52}Cu_{48}$ aerogels was calculated to be 0.960 A mg^{-1}_{Au}, representing a marked enhancement by a factor of 6.3 relative to the Pt/C catalyst (0.153 A mg^{-1}_{Pt}). Remarkably, the SA and MA achieved in the $Au_{52}Cu_{48}$ aerogels are the highest among Au-Cu systems in recently reported studies (Table S3). Figure 3d displays the rotation-rate-dependent LSV curves of $Au_{52}Cu_{48}$ aerogels catalyst. The limiting current increases with an increase of the rotation speed, demonstrating that the ORR catalytic activity of the $Au_{52}Cu_{48}$ aerogels is controlled by the diffusion of O_2.[24] Furthermore, the electron transfer number (n) of the $Au_{52}Cu_{48}$ aerogels catalyst for ORR was calculated to be about 4 from the slopes of the Koutecky-Levich plots (inset in Figure 3d), suggesting a four-electron pathway towards ORR and the complete reduction of O_2 to OH^- on the electrode surface in alkaline media, which is superior to the two-electron peroxide generation process catalyzed by the pure Au (n=2.4) (Figure S6 and S7).

The ORR stability of the catalysts in electrochemical environments is extremely important from a practical viewpoint.[25] Here, the stability of the $Au_{52}Cu_{48}$ aerogels was first evaluated through the accelerated degradation test (ADT), which was performed by applying continuous potential cycling between 0.5 and 1.0 V with a sweep rate of 100 mV s^{-1} in O_2-saturated 0.1 M KOH solution. The commercial Pt/C was used as a baseline catalyst for comparison. As shown in Figure 4a, after 3,000 and 10,000 cycles, the $Au_{52}Cu_{48}$ aerogels catalyst largely retains its ECSA and catalytic activity, showing only 1 and 5 mV negative shifts for the $E_{1/2}$, respectively. The higher ECSA (103.2 m^2 g^{-1}_{Au}), SA (0.891 mA cm^{-2}) and MA (0.920 A mg^{-1}_{Au}) were still well kept after 10,000 potential cycles, which exhibits the only 2.6, 1.7 and 4.2 % decrease compared to the corresponding initial values, respectively (Figure 4c and Table S2). Nevertheless, the commercial Pt/C undergoes a drastic activity decrease after the same durability test.[26] After 10,000 cycles, the Pt/C benchmark catalyst presents a more negative shift of 34 mV in $E_{1/2}$, and its diffusion-limiting current density significantly reduces from 5.87 to 5.15 mA cm^{-2} (Figure 4b). The Pt/C catalyst only retains 46.7, 73.8 and 34.6 % of the original ECSA, SA and MA, respectively (Figure 4c). Most impressively, after the long-term stability test, the $Au_{52}Cu_{48}$ aerogels catalyst still provides 6- and 17-fold enhancements in SA and MA compared with that of Pt/C (0.150 mA cm^{-2} and 0.053 A mg^{-1}_{Pt}, respectively) at 0.85 V. Then, the chronoamperometric (CA) measurement was carried out at 0.82 V in O_2-saturated 0.1 M KOH solution as another forceful support of the $Au_{52}Cu_{48}$ aerogels' outstanding stability. As shown in Figure 4d, the current achieved with the $Au_{52}Cu_{48}$ aerogels catalyst has retained 92 % of its initial value after 40,000 s test, whereas the current on the commercial Pt/C drops to 63 % of the initial value. The aforementioned results from the ADT and CA measurements demonstrate the superior long-term stability of our proposed $Au_{52}Cu_{48}$ aerogels catalyst compared to the commercial Pt/C. The structure and composition evolution of the $Au_{52}Cu_{48}$ aerogels after the stability test (ADT) were further investigated by the TEM analysis. As illustrated in Figure S8, the 3D open architecture of $Au_{52}Cu_{48}$ aerogels is well preserved and the composition change is negligible (Au/Cu ratio changes from 52/48 to 56/44). Therefore, the slower deterioration in ECSA and activity of $Au_{52}Cu_{48}$ aerogels catalyst can be attributed to the stable self-supported nanosponge structures, which significantly mitigates the aggregation, Ostwald ripening of metallic nanoparticles as well as eliminates corrosion problem of the carbon support.[27] Moreover, the existence of Au further facilitates the excellent stability since the superior stabilization effect of Au in the bi/multi-metallic systems has been reported in the literature.[6, 28] The methanol tolerance of the ORR electrocatalysts is another necessary characteristic in terms of the fuel cell's power efficiency.[29] The CA measurement was conducted to examine the possible selectivity and crossover effects of the electrocatalysts. As shown in Figure 4e, the injection of methanol (1 M) induces much slighter responsive current for the $Au_{52}Cu_{48}$ aerogels catalyst, while the current of Pt/C immediately decreases drastically after adding the methanol, indicating that the $Au_{52}Cu_{48}$ aerogels catalyst shows good tolerance toward methanol during catalyzing the ORR process, which has been proved to be the result of its higher selectivity for the ORR rather than the methanol oxidation according to our recently reported study.[8b] Therefore, the $Au_{52}Cu_{48}$ aerogels could be used as a new class of high-performance cathodic ORR electrocatalyst in fuel cells.

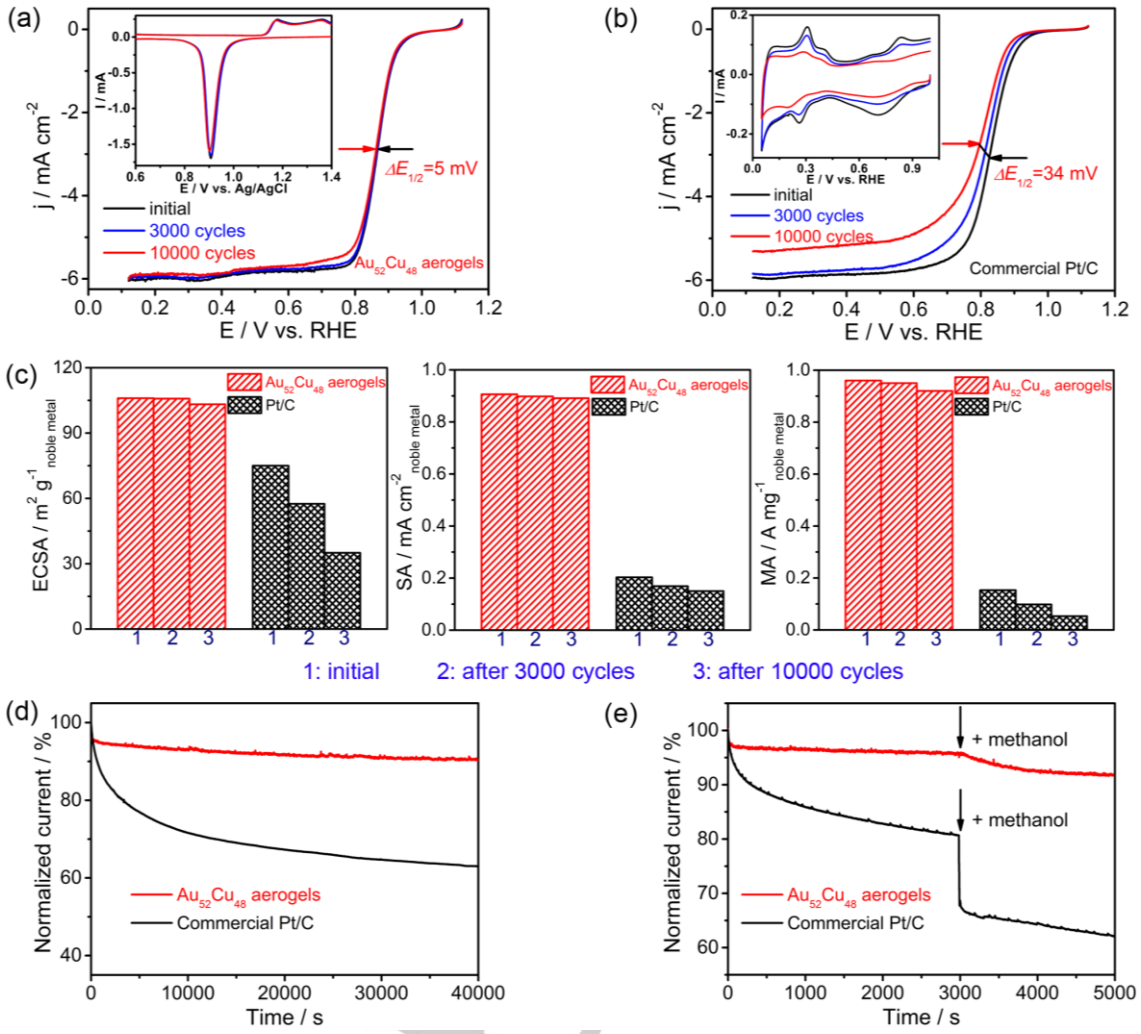

Figure 4. Electrochemical stability and methanol tolerance of the $Au_{52}Cu_{48}$ aerogels and the commercial Pt/C catalysts towards ORR. (a, b) ORR polarization curves and (inset) corresponding CV curves of (a) $Au_{52}Cu_{48}$ aerogels and (b) state-of-the-art commercial Pt/C catalyst before, after 3,000, and after 10,000 potential cycles between 0.5 to 1.0 V vs. RHE. (c) The variations of ECSAs (left), SA (middle) and MA (right) of $Au_{52}Cu_{48}$ aerogels and commercial Pt/C catalysts before, after 3,000, and after 10,000 potential cycles. (d) Chronoamperometric responses (*i-t*) recorded at 0.82 V in O_2-saturated 0.1 M KOH solution at a rotation rate of 1600 rpm for 40,000 s. (e) Methanol crossover test by introducing 1M methanol into the 0.1 M KOH solution at 3000 s (the arrow indicates the addition of methanol).

In addition, the BOR activity of the AuCu aerogels catalysts was also investigated. Figure 5a shows the typical CV curves of $Au_{52}Cu_{48}$ aerogels modified electrode in blank (black dashed line) and 0.1 M sodium borohydride-containing (red solid line) 3 M NaOH solution at a scan rate of 20 mV s^{-1}. In the positive potential sweep, the CV curve exhibits a strong oxidation current peak at 0.54 V, which has been previously reported to originate from the direct oxidation of BH_4^-.[30] The smaller oxidation peak observed around 1.25 V in the reverse potential sweep can be attributed to the oxidation of absorbed borohydroxides as an intermediate. In a sharp contrast, the CV behavior of the Pt/C catalyst for BOR is fairly complex (Figure S9a), which is determined by both catalytic borohydride hydrolysis at more negative potential and the direct BH_4^- oxidation at more positive potential.[30] These results indicate that the $Au_{52}Cu_{48}$ aerogels catalyst shows better selectivity to direct borohydride oxidation versus hydrolysis than that of the Pt/C catalyst. For direct oxidation of BH_4^-, one can see that the $Au_{52}Cu_{48}$ aerogels catalyst obviously outperforms the commercial Pt/C both in the peak potential (0.54 vs. 0.93 V) and the current density (53 vs. 35 mA cm^{-2}). The LSV curves of the electrooxidation of $NaBH_4$ on $Au_{52}Cu_{48}$ aerogels electrode with different rotation rates were shown in Figure 5b. The curves show the typical limiting current plateau at high overpotential, and the currents increase with the increase of rotation rate, indicating that the process of BOR is controlled by the diffusion-convection. The inset in Figure 5b and Figure S9b exhibit the corresponding Koutecky-Levich plots at 1.0 V, from which the apparent number of electrons involved in the direct BH_4^- electrooxidation on $Au_{52}Cu_{48}$ aerogels and Pt/C electrodes can be estimated to be 7.99 and 7, respectively,

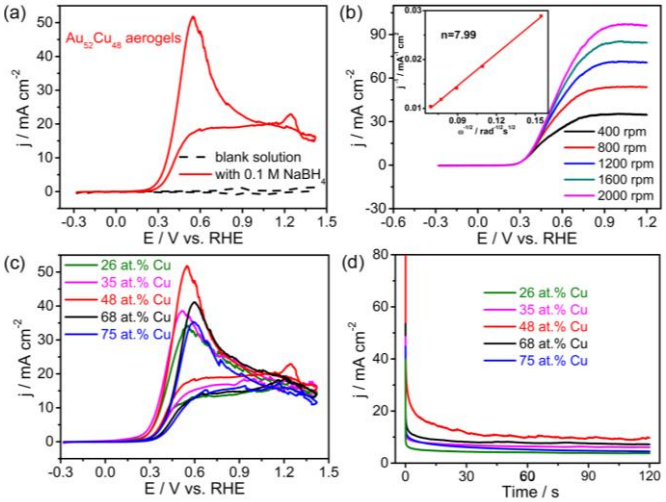

Figure 5. Electrochemical BOR activity of different AuCu aerogels catalysts with various Cu contents. (a) CV curves of $Au_{52}Cu_{48}$ aerogels catalyst recorded in 3 M NaOH blank solution (black dash line) and 0.10 M $NaBH_4$ + 3 M NaOH solution (red solid line) at a scan rate of 20 mV s^{-1}. (b) BOR polarization curves of $Au_{52}Cu_{48}$ aerogels at different rotation rates. The inset shows the corresponding Koutecky-Levich plots (j^{-1} vs. $\omega^{-1/2}$) at 1.0 V and an efficient eight-electron process occur on the $Au_{52}Cu_{48}$ aerogels electrode. (c) CV curves of different AuCu aerogels catalysts recorded 0.10 M $NaBH_4$ + 3 M NaOH solution at a scan rate of 20 mV s^{-1}, indicating the superior BOR activity of $Au_{52}Cu_{48}$ aerogels catalyst among all the AuCu aerogels. (d) Chronoamperometric measurements of borohydride oxidation on different AuCu aerogels in 3M NaOH + 0.1 M $NaBH_4$ solution.

confirming that an efficient eight-electron process is readily to occur on the $Au_{52}Cu_{48}$ aerogels electrode. Impressively, the composition-dependent catalytic activity towards BOR was observed and the $Au_{52}Cu_{48}$ aerogels catalyst possesses the highest activity in terms of more negative onset potential and higher current density (Figure 5c and Figure S10). Most importantly, our proposed $Au_{52}Cu_{48}$ aerogels catalyst is also highly promising among the state-of-the-art BOR electrocatalysts (Table S4), which suggests its great potential as a bifunctional ORR and BOR electrocatalyst for fuel cell technologies. The chronoamperometric responses of the different AuCu aerogels electrodes (potential stepped from -0.28 to 0.72 V) were shown in Figure 5d, all the curves undergo the initial decrease and then reach a practically contant current density with time. It can be found that the $Au_{52}Cu_{48}$ aerogels catalyst has the slowest current decay over time and delivers the highest final current density among all the AuCu aerogels, confirming its excellent BOR electrochemical activity and stability.

In order to reveal the role of the electronic structure onto the catalytic activities, X-ray photoelectron spectroscopy (XPS) was conducted to give detailed analysis of the surface composition and electronic structure for different catalysts. Figure 6a shows the core-level (CL) spectra of Au 4f obtained from different AuCu aerogels and pure Au catalysts. For the $Au_{52}Cu_{48}$ aerogels (red line), two sharp peaks at 84.17 and 87.87 eV were recorded, which are characteristic of spin-orbit splitting (Au $4f_{7/2}$ and Au $4f_{5/2}$, respectively) of Au CL spectra and consistent with the Au^0 chemical state.[31] A close inspection shows that the Au 4f peaks shift to slightly higher binding energies with increasing the Cu content, which is indicative of the gradual incorporation of Cu atoms in the Au and the formation of uniform AuCu bimetallic nanoalloys. In the Cu 2p CL spectrum (Figure 6b), the binding energy values of the Cu $2p_{3/2}$ and Cu $2p_{1/2}$ CLs at 932.6 and 952.3 eV, respectively, are found to be consistent with those reported for metallic Cu.[24, 32] It can be seen that only a trace amount of Cu^{2+} was observed in Cu 2p spectrum, suggesting the effective stabilization effect of Au on Cu, which further confirms the XRD results. The d-band center (ε_d) of different catalysts was then further investigated by the surface valence band spectra (VBS) in Figure 6c. The spectra reveal that the d-band center relative to the Fermi level gradually shifts upwards from pure Au to pure Cu, demonstrating that the electronic structure of the AuCu aerogels can be continuously modulated by nanoalloying with Cu across the entire alloy composition range. According to the design principles well-established on Ag-based catalysts for ORR activity,[33] alloying Ag with higher electronegativity atoms (i.e. Cu) is preferable since withdrawing electrons from Ag to Cu would result in the upshift of d-band center, thus the stronger Ag-O bondings and enhanced ORR catalytic activity. Both Au and Ag atoms lie on the weak binding side of the volcano plot, it is expected, when alloying Au with higher electronegativity atoms, the charge transfer will upshift the d-band center of Au and enhance the catalytic performance of Au-based catalysts. However, based on the VBS spectra, we find that the incorporation of Cu atoms, whose electronegativity is lower than that of Au, does effectively induce an upshift of the d-band center in Au-Cu nanoalloys, indicating that a simple charge transfer effect is inadequate in predicting the shift direction of the d-band center in Au-Cu nanoalloys, which needs further efforts devoted to investigating such intriguing observation.

For a specific transition metal, it is well-known that the more low-lying the d-band center relative to the Fermi level, the weaker the binding energy of reactants/intermediates on the active sites.[34] Accordingly, it is inferred that the binding energy for oxygen on AuCu aerogels catalysts should increase with increasing Cu content. As can be seen in Figure 6d, when the d-band center upshifts from -4.47 to -4.23 eV by increasing Cu content from 0 to 48 at. % in AuCu aerogels, one can see the continuous improvement for the ORR activity. However, the overall ORR catalytic activity trend of all the AuCu aerogels could not exactly follow the linear upshifting relationship with the d-band center approaching to the Fermi level, as shown in Figure 6d and Table S5, the ORR activity is strikingly reversed upon further increasing the Cu content beyond 48 at. %. As discussed, in the lower Cu content regime (< 48 at. %), the continuous incorporation of Cu into the Au efficiently increases the binding of oxygen due to the upshift of d-band center, resulting in the enhanced ORR activity. But furthering the Cu content would lead to the significant decrease of ORR activity, because the oxygen binding energy is so strong to prevent the intermediate desorption. Consequently, the ORR activity follows the volcano shape with a peak activity for $Au_{52}Cu_{48}$ aerogels catalyst (the d-band center upshift of 0.24 eV relative to pure Au),

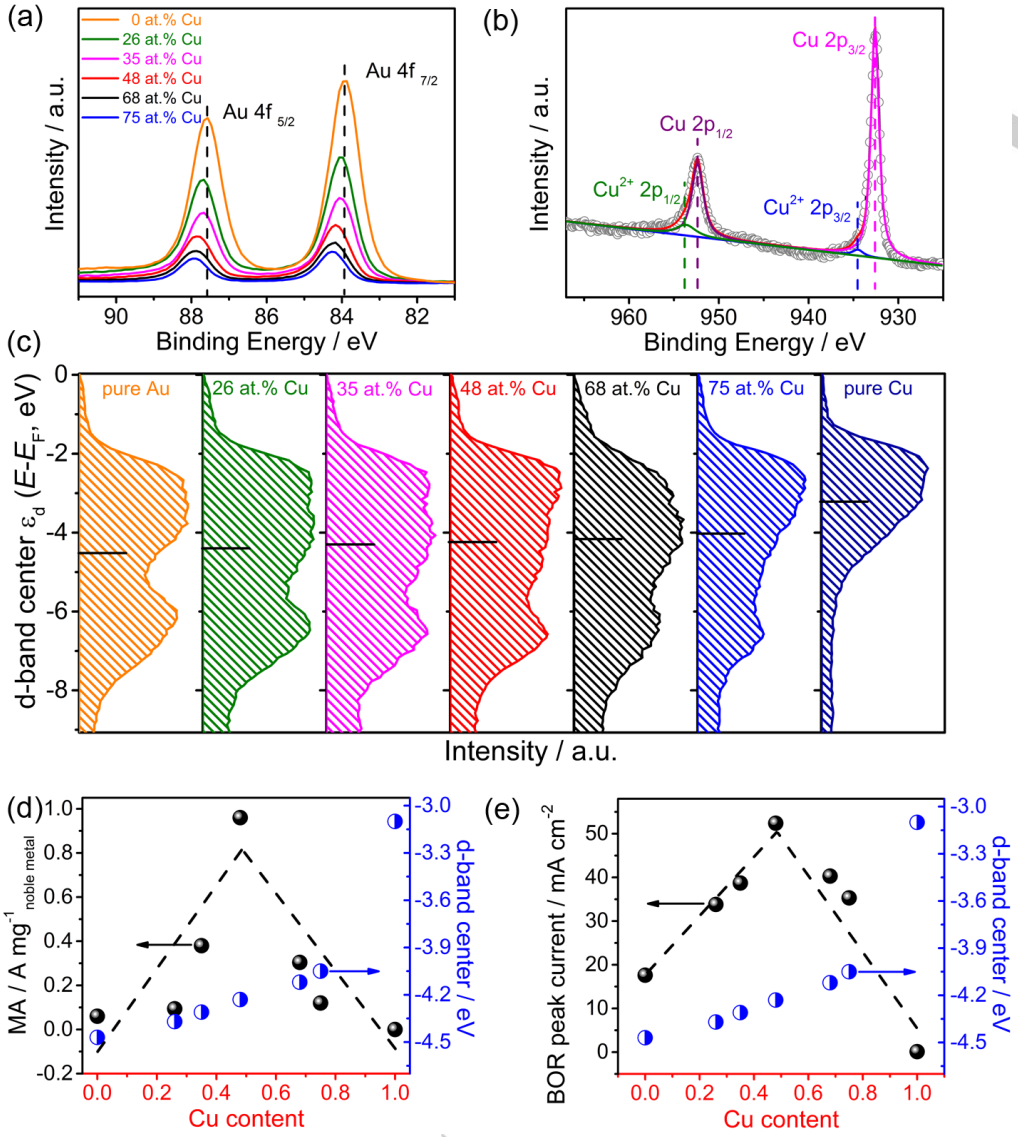

Figure 6. (a) High-resolution spectra of Au 4f region for AuCu aerogels with different Cu contents compared with pure Au, showing clear shift to slightly higher binding energies with increasing the Cu content. (b) High-resolution spectrum of Cu 2p region for $Au_{52}Cu_{48}$ aerogels. (c) Surface Valence Band Spectra (VBS) for the different AuCu aerogels, the black bar indicates its position of d-band center relative to the Fermi level (E-E_F, E, E_F is the energy of the average occupied d-electron density and Fermi energy, respectively), displaying the closer location with respect to the Fermi level with the increase of Cu content. (d) Volcano plots of the ORR activity (mass activity) of the AuCu aerogels catalysts as a function of Cu content and d-band center. (e) Volcano plots of the catalytic BOR activity (peak current density) of the AuCu aerogels catalysts as a function of Cu content and d-band center. Both volcano plots show a peak activity for the $Au_{52}Cu_{48}$ aerogels electrocatalyst.

on which the optimal compromise could be reached between oxygen adsorption and the release of an intermediate. On the other hand, for Pt catalyst, the specific position of the d-band center was calculated and showed in Figure S11, which is located around -2.98 eV. For evaluating the catalytic activity of different metal catalysts, such as AuCu vs. Pt/C catalysts, directly comparing the specific location of their d-band center is not sufficient enough (Table S5). For instance, the half-wave potential of ORR follows the trends: $Au_{52}Cu_{48}$ (d-band center: -4.23 eV) > commercial Pt/C (-2.98 eV) > $Au_{74}Cu_{26}$ (-4.37 eV) > pure Au (-4.47 eV). Previous reports demonstrated that the downshift of d-band center by about 0.1-0.2 eV would achieve the optimal ORR activity for Pt-based catalyst.[1b, 35] While in our research, we find that the $Au_{52}Cu_{48}$ catalyst with the upshift of the d-band center about 0.24 eV exhibits the highest ORR activity. The favorable shift of the d-band center in different catalysts would facilitate to achieve optimal catalytic activity. Therefore, we provided the optimal upshift value of the d-band center for catalytic reactions in the as-synthesized AuCu aerogels, which is more important to accurately predict trends in the catalytic activity and guide the design of novel bi/multi-metallic electrocatalysts.

More interestingly, as shown in Figure 6e, a similar composition-dependent volcano shape trend for the catalytic BOR activity with a peak activity for $Au_{52}Cu_{48}$ aerogels was also observed, which can be understood in terms of the same electronic effect according to the aforementioned analysis. The moderate upshift of the d-band center might lead to the stronger molecular adsorption of BH_4^- on the AuCu aerogels surface and then facilitate the B-H dissociation,[36] moreover, the simultaneously resulting stronger adsorption of OH^- species further favor the direct BH_4^- oxidation.[37] Previous DFT calculations suggested that the combination site of Au and Cu rather than Au-Au or Cu-Cu site would provide the higher catalytic activities.[37-38] Herein, the atomic ratio of Au/Cu ~ 52/48 in AuCu aerogels is believed to reflect an optimal atomic-scale alloying effect of Cu atoms surrounding Au atoms. The high fraction of Au-Cu contacts would be highly beneficial to create the strong electronic effect and ensure the entire catalyst experiences the d-band shift to achieve higher catalytic activities.[39] Based on the physical and electrochemical characterizations, the unprecedented performance enhancement on the AuCu aerogels catalyst for both ORR and BOR is believed to originate from the combination of the robust electronic structure and the high specific surface area. These two factors affect the catalytic activities from different aspects. The electronic effect could effectively modulate the binding energy of reactants molecules on the AuCu catalysts surface and then facilitate the catalytic kinetics. While the high specific surface area could expose more active sites (as manifested in the larger ECSA) and favor the accessibility of reactants molecules to the active sites, further enhancing the electrocatalytic activities. Such high performance AuCu aerogels catalyst not only shows great potential to be a promising alternative for Pt-based electrocatalyst but also shines some light on the design of more efficient and developed electrocatalysts for sustainable energy applications.

Conclusions

In summary, a new class of self-assembled AuCu aerogels was synthesized via a one-step kinetically-controlled approach with 3D open architecture and well-controlled composition at room temperature. XPS spectra reveal that the uniformly-distributed Cu atoms can effectively upshift the d-band center in Au-Cu aerogels within the entire alloy composition range, importantly activating the catalytic sites for higher performance. Due to the unexpected electronic effect and the favorable porous architecture, the $Au_{52}Cu_{48}$ aerogels with the optimal d-band center upshift (0.24 eV relative to pure Au) exhibit remarkably enhanced catalytic performance for both ORR and BOR compared with the commercial state-of-the-art Pt/C catalysts in alkaline solution, and also show the highest activity among the current Au-Cu systems. Most impressively, the $Au_{52}Cu_{48}$ aerogels achieve extraordinary long-term durability for ORR, as confirmed by the harsh potential cycling (10,000 cycles) and chronoamperometric measurement (40,000 s), showing great potential possibility in real fuel cell devices. In addition, the synthetic strategy to prepare AuCu aerogels is general and versatile, which can be extended to synthesize other bi/multi-metallic systems with varying chemical composition. The intriguing synergetic effect reported in this work paves a new pathway for engineering novel nanoalloys with tunable structural and electronic properties to serve as the efficient electrocatalysts for next-generation fuel cells.

Experimental Section

Synthesis of AuCu, pure Au and pure Cu aerogels

In a typical synthesis of $Au_{52}Cu_{48}$ aerogels, 4 mL of metal precursor solution containing 0.025 M $HAuCl_4$ and 0.025 M $CuCl_2$ was quickly injected to 20 mL of an aqueous solution of 0.1 M $NaBH_4$ (1:5, v/v ratio of metal precursor/$NaBH_4$ solution) with stirring at room temperature. The resultant solution was kept stirring for about three minutes until the entire solution became colorless, and then allowed to settle still at room temperature without fluctuation. The rapid kinetically-controlled reduction reaction between metal cations and strong reduction agent resulted in the fast formation of black spongy solid, which vigorously floated up and down with the aid of effervescence (due to the release of H_2). After few minutes, the obtained $Au_{52}Cu_{48}$ aerogels were washed thoroughly with water for three times and then freeze-dried overnight. In a similar method, $Au_{74}Cu_{26}$, $Au_{65}Cu_{35}$, $Au_{32}Cu_{68}$, and $Au_{25}Cu_{75}$ aerogels were synthesized by simply adjusting the concentration of metal precursors (Table S1). For comparison, pure monometallic Au and Cu aerogels were also synthesized by adding 4 mL of 0.025 M metal precursor solution into 20 mL of 0.1 M $NaBH_4$ solution. The single $HAuCl_4$ and $CuCl_2$ were used as the precursors for synthesis of pure Au and pure Cu aerogels, respectively. To ensure the reproducibility of each sample, we fabricated at least three separated samples for each kind of catalyst.

Characterizations

All the transmission electron microscopy (TEM) and high-resolution TEM (HRTEM) images were conducted by using a FEI Tecnai F30 microscopy with the accelerating voltage of 200 kV. Scanning electron microscopy (SEM) was performed on a FEI NovaSEM 450 field emission scanning electron microscope. The powder X-ray diffraction (XRD) measurement was obtained on the PANalytical X'Pert Pro MPD with Cu Kα radiation (λ = 1.5406 Å). X-ray photoelectron spectroscopy (XPS) characterization was performed on an ESCALAB 250 instrument under ultrahigh vacuum (10^{-9} Torr) by using monochromated Al Kα radiation (hv = 1486.6 eV), all the binding energy were calibrated by the carbon peak (C 1s) at about 284.5 eV. The d-band center positions were calculated according to the formula in the range of 0 and -9 eV: $\int N(\varepsilon)\varepsilon d\varepsilon$ / $\int N(\varepsilon)d\varepsilon$, where $N(\varepsilon)$ is the density of states (DOS), and all the spectra collected are corrected using the Shirley background,[40] and the standard deviation of the calculated values is 0.012. Nitrogen physisorption isotherms were measured with ASAP 2460 at liquid nitrogen temperature (77K).

Electrochemical measurements

Electrochemical measurements were performed in a standard three-electrode cell with the CHI 660C electrochemical workstation (Shanghai Chenhua Apparatus, China) at room temperature. Glassy carbon rotating disk electrode (GCE, diameter: 5 mm, area: 0.196 cm^2) from Pine Instruments, as the working electrode, was successively polished with 0.3 and 0.05 μm alumina slurry and ultrasonically cleaned in acetone and ultrapure water before the surface coating. To prepare the working

electrode, the as-synthesized AuCu aerogels were dispersed ultrasonically in a mixture of ethanol and Nafion solution to form a catalyst ink. Afterwards, about 10 μL of the dispersion was deposited onto the surface of a glassy carbon electrode. Then, the electrode was allowed to dry naturally. The Au loading of different AuCu aerogels were all 25.5 μg_{Au} cm^{-2}. For comparison, the commercial Pt/C catalyst was used as the baseline catalysts (Pt loading 20 wt. % from Johnson Matthey, fuel cell grade), and the same procedure was used to form the Pt/C ink, and the Pt loading was 20.4 μg_{Pt} cm^{-2}.

For the oxygen reduction reactions (ORR), the electrolyte solution of 0.1 M KOH was prepared from ultrapure water and potassium hydroxide. The catalyst covered GCE, platinum wire, mercury-mercury oxide (MMO) Hg|HgO|(NaOH 1M) were used as the working electrode, counter electrode and reference electrode, respectively. All potential values in this paper were referred to the reversible hydrogen electrode (RHE) unless otherwise stated. All electrochemical measurements were carried out at room temperature using research-grade gases. Cyclic voltammograms (CVs) were taken in N_2-saturated 0.1 M KOH solution, and linear sweep voltammetry (LSV) curves were measured at the different rotation rate (400, 800, 1200, 1600 and 2000 rpm) in O_2-saturated 0.1 M KOH solution. The following equation (Koutecky-Levich equation, j^{-1} versus $\omega^{-1/2}$) was used to estimate the ORR selectivity to H_2O or H_2O_2 ($4e^-$ and $2e^-$ reduction): $j^{-1} = j_k^{-1} + 1/(0.62nFC_0D_0^{2/3}v^{-1/6}\omega^{1/2})$, where j is the actual current density, j_k is the kinetic current density, n denotes the overall electron transfer number in oxygen reduction, F is the Faraday constant (96485 C mol^{-1}), C_0 represents the bulk concentration of O_2 (1.2×10^{-6} mol cm^{-3}), D_0 is the diffusion coefficient of O_2 (1.9×10^{-5} cm^2 s^{-1}) in 0.1 M KOH aqueous solution, v represents the kinetic viscosity of the electrolyte (0.01 cm^2 s^{-1}), and ω is the angular velocity of the RDE ($\omega = 2\pi N$, N is the linear rotation speed in rpm). The ORR stability was recorded by the accelerated degradation test (ADT) and chronoamperometric (CA) measurement. Specifically, ADT test was performed by applying continuous potential cycling between 0.5 and 1.0 V with a sweep rate of 100 mV s^{-1} in O_2-saturated 0.1 M KOH solution for 10,000 cycles. CA measurement (*i-t* curve) was carried out at 0.82 V in O_2-saturated 0.1 M KOH solution for 40,000 s. The methanol tolerance test was performed by introducing methanol into the O_2-saturated 0.1 M KOH solution (1 M methanol) at 3,000 s during the CA measurement.

For the borohydride oxidation reaction (BOR), the cyclic voltammograms (CVs) and linear scan voltammograms (LSVs) were recorded at a scan rate of 20 mV s^{-1}, the electrode rotation speed differed from 400 to 2000 rpm. The chronoamperometry (CA) curve was taken by the potential step from - 0.28 to 0.72 V. The electrolyte was 3 M NaOH + 0.1 M $NaBH_4$ for CV tests. The Koutecky-Levich equation stated above was also used to estimate the electron transfer number during the BOR process, where C_0 is the bulk concentration of BH_4^-, D_0 is the BH_4^- diffusion coefficient (1.6×10^{-5} cm^2 s^{-1}), v represents the kinetic viscosity of the electrolyte (1.19×10^{-2} cm^2 s^{-1}).

The electrochemically active surface areas (ECSAs) of AuCu aerogels and commercial Pt/C catalysts were calculated from the corresponding CVs in N_2-saturated solutions. The typical CV curve of AuCu aerogels was carried out in 0.5 M H_2SO_4 solution, then the ECSA was further determined by measuring the charge collected in the region of Au oxide reduction and assuming the charge density of 390 μC cm^{-2}. The ECSA of the commercial Pt/C was evaluated from the CV curve recorded in 0.1 M KOH solution by integrating the charge in the hydrogen adsorption/desorption region, assuming a value of 210 μC cm^{-2} for the adsorption of a hydrogen monolayer.

Acknowledgements

This work was supported by the National Natural Science Foundation of China (grant nos. 51271148 and 50971100), the Research Fund of State Key Laboratory of Solidification Processing in China (grant no. 150-ZH-2016), the Aeronautic Science Foundation Program of China (grant no. 2012ZF53073), the Project of Transformation of Scientific and Technological Achievements of NWPU (grant no. 19-2017), the Doctoral Fund of Ministry of Education of China (grant no. 20136102110013), and the Open Fund of State Key Laboratory of Advanced Technology for Materials Synthesis and Processing (Wuhan University of Technology, grant no. 2018-KF-18).

Keywords: one-pot approach • electronic modulation • oxygen reduction • borohydride oxidation • alternative for Pt-based catalyst

[1] a) S. Chu, Y. Cui, N. Liu, *Nat. Mater.* **2017**, *16*, 16-22; b) C. Meng, T. Ling, T. Y. Ma, H. Wang, Z. Hu, Y. Zhou, J. Mao, X. W. Du, M. Jaroniec, S. Z. Qiao, *Adv. Mater.* **2017**, *29*, 1604607.

[2] V. R. Stamenkovic, D. Strmcnik, P. P. Lopes, N. M. Markovic, *Nat. Mater.* **2017**, *16*, 57-69.

[3] a) N. Zhang, Y. Feng, X. Zhu, S. Guo, J. Guo, X. Huang, *Adv. Mater.* **2017**, *29*, 1603774; b) X. Ge, A. Sumboja, D. Wuu, T. An, B. Li, F. T. Goh, T. A. Hor, Y. Zong, Z. Liu, *ACS Catal.* **2015**, *5*, 4643-4667.

[4] a) V. R. Stamenkovic, B. Fowler, B. S. Mun, G. Wang, P. N. Ross, C. A. Lucas, N. M. Marković, *science* **2007**, *315*, 493-497; b) P. Hu, Y. Song, L. Chen, S. Chen, *Nanoscale* **2015**, *7*, 9627-9636; c) B. Wang, *J. Power Sources* **2005**, *152*, 1-15.

[5] a) X. Huang, Z. Zhao, L. Cao, Y. Chen, E. Zhu, Z. Lin, M. Li, A. Yan, A. Zettl, Y. M. Wang, *Science* **2015**, *348*, 1230-1234; b) L. Bu, S. Guo, X. Zhang, X. Shen, D. Su, G. Lu, X. Zhu, J. Yao, J. Guo, X. Huang, *Nat. Commun.* **2016**, *7*, 11850; c) Y. Jang, K.-H. Choi, D. Y. Chung, J. E. Lee, N. Jung, Y.-E. Sung, *ChemSusChem* **2017**, *10*, 3063-3068.

[6] J. Zhang, K. Sasaki, E. Sutter, R. Adzic, *Science* **2007**, *315*, 220-222.

[7] a) H. Yin, H. Tang, D. Wang, Y. Gao, Z. Tang, *ACS Nano* **2012**, *6*, 8288-8297; b) A. Wittstock, V. Zielasek, J. Biener, C. Friend, M. Bäumer, *Science* **2010**, *327*, 319-322.

[8] a) J. Wang, F. Chen, Y. Jin, R. L. Johnston, *J. Mater. Chem. A* **2016**, *4*, 17828-17837; b) J. Wang, F. Chen, Y. Jin, Y. Lei, R. L. Johnston, *Adv. Funct. Mater.* **2017**, *27*, 1700260.

[9] H.-B. Noh, M. H. Naveen, Y.-J. Choi, E. S. Choe, Y.-B. Shim, *Chem. Commun.* **2015**, *51*, 6659-6662.

[10] C. L. Bracey, P. R. Ellis, G. J. Hutchings, *Chem. Soc. Rev.* **2009**, *38*, 2231-2243.

[11] a) D. Wen, W. Liu, D. Haubold, C. Zhu, M. Oschatz, M. Holzschuh, A. Wolf, F. Simon, S. Kaskel, A. EychmüLler, *ACS Nano* **2016**, *10*, 2559-2567; b) S. Pedireddy, H. K. Lee, W. W. Tjiu, I. Y. Phang, H. R. Tan, S. Q. Chua, C. Troadec, X. Y. Ling, *Nat. Commun.* **2014**, *5*, 4947.

[12] a) D. Kim, C. Xie, N. Becknell, Y. Yu, M. Karamad, K. Chan, E. J. Crumlin, J. K. Norskov, P. Yang, *J. Am. Chem. Soc.* **2017**, *139*, 8329-8336; b) Z. Xu, E. Lai, Y. Shao-Horn, K. Hamad-Schifferli, *Chem. Commun.* **2012**, *48*, 5626-5628.

[13] J. Wang, H. Zhu, D. Yu, J. Chen, J. Chen, M. Zhang, L. Wang, M. Du, *ACS Appl. Mater. Interfaces* **2017**, *9*, 19756-19765.

[14] a) S. Najafishirtari, R. Brescia, P. Guardia, S. Marras, L. Manna, M. Colombo, *ACS Catal.* **2015**, *5*, 2154-2163; b) S.-I. Kim, G. Eom, M. Kang, T. Kang, H. Lee, A. Hwang, H. Yang, B. Kim, *Nanotechnology* **2015**, *26*, 245702.

[15] a) G. Wang, B. Huang, L. Xiao, Z. Ren, H. Chen, D. Wang, H. D. Abruña, J. Lu, L. Zhuang, *J. Am. Chem. Soc.* **2014**, *136*, 9643-9649; b) G. Wang, J. Guan, L. Xiao, B. Huang, N. Wu, J. Lu, L. Zhuang, *Nano Energy* **2016**, *29*, 268-274; c) J. Yang, X. Chen, X. Yang, J. Y. Ying,

Energy Environ. Sci. **2012**, *5*, 8976-8981.

[16] G. Wang, L. Xiao, B. Huang, Z. Ren, X. Tang, L. Zhuang, J. Lu, *J. Mater. Chem.* **2012**, *22*, 15769-15774.

[17] N. Zhang, X. Chen, Y. Lu, L. An, X. Li, D. Xia, Z. Zhang, J. Li, *Small* **2014**, *10*, 2662-2669.

[18] a) B. Cai, D. Wen, W. Liu, A.-K. Herrmann, A. Benad, A. Eychmüller, *Angew. Chem. Int. Ed.* **2015**, *54*, 13101-13105; b) K. G. S. Ranmohotti, X. Gao, I. U. Arachchige, *Chem. Mater.* **2013**, *25*, 3528-3534.

[19] K. S. Krishna, C. S. Sandeep, R. Philip, M. Eswaramoorthy, *ACS Nano* **2010**, *4*, 2681-2688.

[20] a) A. Wittstock, M. Bäumer, *Acc. Chem. Res* **2014**, *47*, 731-739; b) H. Liu, Q. Yang, *J. Mater. Chem.* **2011**, *21*, 11961-11967.

[21] W. Liu, P. Rodriguez, L. Borchardt, A. Foelske, J. Yuan, A. K. Herrmann, D. Geiger, Z. Zheng, S. Kaskel, N. Gaponik, *Angew. Chem. Int. Ed.* **2013**, *52*, 9849-9852.

[22] A.-K. Herrmann, P. Formanek, L. Borchardt, M. Klose, L. Giebeler, J. R. Eckert, S. Kaskel, N. Gaponik, A. EychmüLler, *Chem. Mater.* **2013**, *26*, 1074-1083.

[23] V. M. Dhavale, S. Kurungot, *ACS Catal.* **2015**, *5*, 1445-1452.

[24] Y. Jin, F. Chen, Y. Lei, X. Wu, *ChemCatChem* **2015**, *7*, 2377-2383.

[25] J. Li, H.-M. Yin, X.-B. Li, E. Okunishi, Y.-L. Shen, J. He, Z.-K. Tang, W.-X. Wang, E. Yücelen, C. Li, *Nature Energy* **2017**, *2*, 17111.

[26] A. Zadick, L. Dubau, N. Sergent, G. Berthome, M. Chatenet, *ACS Catal.* **2015**, *5*, 4819-4824.

[27] Z. Chen, M. Waje, W. Li, Y. Yan, *Angew. Chem. Int. Ed.* **2007**, *46*, 4060-4063.

[28] X. Sun, D. Li, Y. Ding, W. Zhu, S. Guo, Z. L. Wang, S. Sun, *J. Am. Chem. Soc.* **2014**, *136*, 5745-5749.

[29] U. Din, M. Aizaz, F. Saleem, B. Ni, Y. Yong, X. Wang, *Adv. Mater.* **2017**, *29*, 1604994.

[30] E. Gyenge, *Electrochim. Acta* **2004**, *49*, 965-978.

[31] M. H. Naveen, N. G. Gurudatt, H. B. Noh, Y. B. Shim, *Adv. Funct. Mater.* **2016**, *26*, 1590-1601.

[32] a) J. Yin, S. Shan, L. Yang, D. Mott, O. Malis, V. Petkov, F. Cai, M. Shan Ng, J. Luo, B. H. Chen, *Chem. Mater.* **2012**, *24*, 4662-4674; b) Y. Jin, F. Chen, *Electrochim. Acta* **2015**, *158*, 437-445.

[33] X. Wu, F. Chen, N. Zhang, Y. Lei, Y. Jin, A. Qaseem, R. L. Johnston, *Small* **2017**, *13*, 1603387.

[34] J. K. Nørskov, T. Bligaard, J. Rossmeisl, C. H. Christensen, *Nat. Chem.* **2009**, *1*, 37-46.

[35] V. Stamenkovic, B. S. Mun, K. J. Mayrhofer, P. N. Ross, N. M. Markovic, J. Rossmeisl, J. Greeley, J. K. Nørskov, *Angew. Chem.* **2006**, *118*, 2963-2967.

[36] A. M. Pasqualeti, P.-Y. Olu, M. Chatenet, F. H. Lima, *ACS Catal.* **2015**, *5*, 2778-2787.

[37] G. Rostamikia, M. J. Janik, *Energy Environ. Sci.* **2010**, *3*, 1262-1274.

[38] N. Zhang, H. Yan, X. Chen, L. An, Z. Xia, D. Xia, *J. Phys. Chem. C* **2015**, *119*, 907-912.

[39] D. A. Slanac, W. G. Hardin, K. P. Johnston, K. J. Stevenson, *J. Am. Chem. Soc.* **2012**, *134*, 9812-9819.

[40] S. J. Hwang, S.-K. Kim, J.-G. Lee, S.-C. Lee, J. H. Jang, P. Kim, T.-H. Lim, Y.-E. Sung, S. J. Yoo, *J. Am. Chem. Soc.* **2012**, *134*, 19508-19511.

Entry for the Table of Contents

FULL PAPER

We proposed a new class of self-assembled AuCu aerogels through a one-pot kinetically-controlled strategy. The startling electronic modulation effect of Cu on Au was observed across the entire composition range. The AuCu aerogels exhibited extraordinary activity and durability for the oxygen reduction and borohydride oxidation reactions in alkaline media, serving as the promising alternative for Pt-based catalyst in fuel cells.

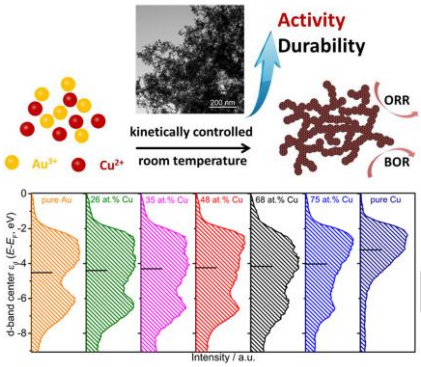

Jiali Wang, Fuyi Chen, Yachao Jin, and Roy L. Johnston*

Page 1 – Page 11

AuCu Aerogels with Intriguing Surface Electronic Modulation as Highly Active and Stable Electrocatalysts for Oxygen Reduction and Borohydride Oxidation